

STRUCTURE AND EVOLUTION OF ZEL'DOVICH PANCAKES AS PROBES OF DARK ENERGY MODELS

P. M. SUTTER

Department of Physics, University of Illinois at Urbana-Champaign, Urbana, IL 61801-3080

AND

P. M. RICKER

Department of Astronomy, University of Illinois at Urbana-Champaign, Urbana, IL 61801
 National Center for Supercomputing Applications, University of Illinois at Urbana-Champaign, Urbana, IL 61801
Draft version February 14, 2008

ABSTRACT

We examine how coupled dark matter and dark energy modify the development of Zel'dovich pancakes. We study how the various effects of these theories, such as a fifth force in the dark sector and a modified particle Hubble drag, produce variations in the redshifts of caustic formation and the present-day density profiles of pancakes. We compare our results in direct simulation to a perturbation theory approach for the dark energy scalar field. We determine the range of initial scalar field amplitudes for which perturbation theory is accurate in describing the development of the pancakes. Notably, we find that perturbative methods which neglect kinetic terms in the scalar field equation of motion are not valid for arbitrarily small perturbations. We also examine whether models that have been tuned to match the constraints of current observations can produce new observable effects in the nonlinear structure of pancakes. Our results suggest that a fully realistic three-dimensional simulation will produce significant new observable features, such as modifications to the mass function and halo radial density profile shapes, that can be used to distinguish these models from standard concordance cosmology and from each other.

Subject headings: cosmology:theory, dark matter, dark energy, structure formation, methods: N-body simulations

1. INTRODUCTION

Dark energy is perhaps the most profound and essential mystery in modern cosmology. While the Λ CDM cosmological model has proven very successful in explaining and predicting many features of our universe, such as the fluctuations in the cosmic microwave background (eg. de Bernardis et al. 2000), the large-scale matter distribution (eg. Percival et al. 2001), and distance measurements to type Ia supernovae (Perlmutter et al. 1999; Riess et al. 1998), the physics of the dark sector (dark matter and dark energy), which comprises roughly ninety-six percent of the energy density of the universe, is largely unknown.

Currently, there are too few observational constraints to determine the precise nature of the dark energy and any possible interactions it might have with dark and baryonic matter (Bean et al. 2005). However, we can use simulations of nonlinear structure formation to explore the consequences of plausible dark energy models, including those that propose couplings between dark matter (DM) and dark energy (DE) (see Alcaniz 2006, and references therein). Models that have particle physics motivations often predict such couplings (Amendola 2000). Such theories are intriguing because they might provide a resolution to current cosmological problems, such as the so-called coincidence problem (Zimdahl & Pavon 2001; Amendola & Tocchini-Valentini 2001), and the observed emptiness of the voids (Farrar & Peebles 2004), the latter of which was confirmed numerically by Nusser, Gubser, & Peebles (2005).

An important goal of coupled DM-DE simulations is to identify observational methods to test these theories. The observables studied to date include luminosity distances (Amendola et al. 2007), the growth of matter perturbations (Olivares et al. 2006; Koivisto 2005), the abundance of clusters (Manera & Mota 2006), and the Sandage-Loeb test (Corasaniti et al. 2007). Not only can we use such simulations to search for additional observable features, but we can also use them to find ways to distinguish models and determine the validity of perturbation methods.

Much of the work to date has followed the framework established by Farrar & Peebles (2004). This model uses a dynamical scalar field to provide the dark energy, and it allows that field to couple to dark matter via a Yukawa interaction. Although there are some issues with models of this type (Doran & Jäkel 2002), they provide useful foils for studying the possible effects that other models, which are complicated but more robust, might predict. These models would include the model discussed by Huey & Wandelt (2006) and the two-family model considered in Farrar and Peebles.

Some of the previous work has examined structure formation with modifications due to a fifth force, albeit at low spatial and force resolution (Nusser et al. 2005; Macciò et al. 2004). However, we believe that an incremental approach that analyzes the various effects of DM-DE interactions on simpler initial conditions is crucial before tackling more realistic initial conditions. This approach allows the effects observed in more realistic simulations to be understood and generalized. Therefore, in this paper, we will study the effects of coupling between dark matter and dark energy

on the development of Zel'dovich pancakes. Zel'dovich pancakes are the well-known solutions to the problem of the gravitational collapse of one-dimensional, sinusoidal, plane-wave, adiabatic density perturbations (Zel'dovich 1970). Since they are well-studied in a variety of contexts not involving DM-DE interactions (for example, More 1988; Gnedin 1993; Yuan et al. 1991; Valinia et al. 1995; Anninos & Norman 1994; Anninos et al. 1995, and others), we can more easily understand the effects of additional physics on structure formation, laying the groundwork for a more complete three-dimensional study.

In Section 2 we discuss the relevant equations, the effects we will study, and our numerical techniques. Section 3 discusses the role that the exotic physics introduced by the Farrar and Peebles model, such as a DM particle fifth force and time-dependent DM particle mass, plays in structure formation. We are careful to separate the various effects predicted by the model. Even if this particular example does not withstand closer scrutiny, unrelated theories may predict similar effects.

In addition, so far many researchers have exploited perturbation theory to treat fluctuations in the DE scalar field. However, we do not know *a priori* the validity of this approach, especially as we begin to explore the nonlinear consequences of this theory. In Section 4 we will compare the structure formation results from perturbation theory alone to the results from doing a complete nonlinear analysis. We will also discuss the regime where perturbation theory is most valid in accurately predicting structure.

Many of the theories of this type have adjustable parameters, and these parameters must be adjusted to match Λ CDM predictions, at the risk of being indistinguishable from it. There are also usually several unique combinations of parameters that provide similar, if not identical, results. In Section 5 we attempt to find ways to distinguish models that remain indistinct in perturbation theory. Also, we will determine if nonlinear effects can distinguish models from standard cosmology even when effects based on perturbative methods cannot.

2. THE MODEL

2.1. Coupled Dark Matter and Dark Energy

Following Farrar and Peebles, we will consider a dark energy (DE) scalar field ϕ with action

$$S_{DE} = \int d^4x \sqrt{-g} \left[\frac{1}{2} \phi_{,\nu} \phi^{,\nu} - V(\phi) \right], \quad (1)$$

and a single classical nonrelativistic dark matter (DM) particle family with action for the i th particle

$$S_{DMi} = - \int y |\phi(x_i) - \phi_*| \sqrt{g_{\mu\nu} dx_i^\mu dx_i^\nu}, \quad (2)$$

where y is the dimensionless Yukawa interaction strength and ϕ_* is a constant providing an intrinsic mass to the DM particle. We will set $\phi_* = 0$, so that the DM particle mass is due entirely to the field value. In both of the above actions and throughout, we have set $\hbar = c = 1$, and we will ignore baryons.

Assuming a spatially flat Friedmann universe, we can use equation (2) to obtain a comoving DM particle equation of motion in one dimension:

$$\dot{v} + \left(2 \frac{\dot{a}}{a} + \frac{\dot{\phi}}{\phi} \right) v = - \frac{\partial \Phi}{\partial x} - \frac{1}{a^2} \frac{1}{\phi} \frac{\partial \phi}{\partial x}. \quad (3)$$

Here, Φ is the normal comoving gravitational potential, a is the scale factor, and v is the comoving particle velocity, and x is the comoving position. Throughout, dots refer to derivatives with respect to proper time t . The field action in equation (1) gives the evolution of ϕ :

$$\ddot{\phi} - \frac{1}{a^2} \nabla^2 \phi + 3 \frac{\dot{a}}{a} \dot{\phi} + \frac{dV}{d\phi} + \frac{\rho}{\phi} a^{-3} = 0, \quad (4)$$

where ρ is the DM particle comoving density.

The comoving potential satisfies the Poisson equation:

$$\nabla^2 \Phi = \frac{4\pi G}{a^3} (\rho - \bar{\rho}). \quad (5)$$

Here and throughout, an overline indicates a spatial average.

The Friedmann equation, neglecting radiation, curvature, and baryonic terms, is now

$$\left(\frac{\dot{a}}{a} \right)^2 = H_0^2 \Omega_m \frac{\bar{\phi}}{\phi_0} a^{-3} + \frac{8\pi G}{3} \left[\frac{1}{2} \left(\frac{d\bar{\phi}}{dt} \right)^2 + V(\bar{\phi}) \right]. \quad (6)$$

A subscript of 0 denotes the present-day value. The first term on the right-hand side reflects the contribution of the DM with its time-dependent mass. The terms in brackets are, respectively, the kinetic and potential energies of the DE scalar field.

We do not know the initial conditions of the field, but we do know that today the field behaves as a cosmological constant, so the potential term dominates and has a value

$$V(\bar{\phi}_0) = \Omega_\Lambda \rho_{crit}. \quad (7)$$

Also, at early enough times, Farrar and Peebles found that equation (4) reduces to

$$\frac{d\phi}{dt} = - \frac{H_0^2}{G} \frac{3\Omega_m}{8\pi\phi_0} \frac{1}{a^3} t, \quad (8)$$

which we use to set the initial condition for $\dot{\phi}$.

We can identify four unique ways in which the extra interactions modify structure formation. First, the DM particle mass directly depends on the field value, so we may write the ratio of the modified mass to its present-day value as

$$\eta \equiv \frac{m_{DM}}{m_{DM,0}} = \frac{\phi}{\phi_0} \quad (9)$$

Secondly, the interactions modify the Hubble drag found in the DM equation of motion, so that its ratio to the drag in standard cosmology is

$$\gamma \equiv \frac{2\dot{a}/a + \dot{\phi}/\phi}{2\dot{a}/a}. \quad (10)$$

Next, we notice a modified particle acceleration due to a fifth force in equation (3). We will define

$$\beta \equiv \frac{\frac{\partial \Phi}{\partial x} + \frac{1}{a^2} \frac{1}{\phi} \frac{\partial \phi}{\partial x}}{\frac{\partial \Phi}{\partial x}}. \quad (11)$$

Finally, the dynamic scalar field itself indirectly affects structure formation via a time-varying Ω_Λ in the Friedmann equation. We define

$$\delta \equiv \frac{\frac{1}{2} \left(\frac{d\bar{\phi}}{dt} \right)^2 + V(\bar{\phi})}{V(\bar{\phi}_0)}. \quad (12)$$

If the fluctuations in the field are small enough, we may do perturbation theory. Farrar and Peebles found that in this regime, we may replace $\phi(x)$ with a single spatial average, ϕ_b and a sufficiently small perturbation field $\phi_1(x)$. We may then write equation (4) as

$$\ddot{\phi}_b + 3\frac{\dot{a}}{a}\dot{\phi}_b + \frac{dV}{d\phi_b} + \frac{3\Omega_m H_0^2}{8\pi G\phi_{b,0}}a^{-3} = 0. \quad (13)$$

Also, the fifth force ratio appears instead as

$$\beta_{pert} \equiv 1 + \frac{1}{4\pi G\phi_b^2}. \quad (14)$$

We will contrast our results with standard concordance cosmology, which we achieve by setting ϕ to a single value satisfying equation (7) and by preventing ϕ from evolving dynamically.

We have the freedom to choose an appropriate potential $V(\phi)$. Although there are many potentials in the literature, such as the exponential (Ratra & Peebles 1988), power-law (Peebles & Ratra 1988), and power-law and sine (Dodelson et al. 2000), we will adopt the power-law potential found in Farrar and Peebles:

$$V(\phi) = K/\phi^\alpha, \quad (15)$$

where we are also free to choose the constants K and α . Potentials like this lead to reasonable behavior, i.e. potential-dominated solutions at the present epoch. Again, we chose this potential merely as an example.

2.2. Numerical Techniques

For our simulations we developed a one-dimensional N -body particle-mesh code. We used cloud-in-cell mapping for interpolating between the mesh and particles (Hockney & Eastwood 1988), and a second order leapfrog integration scheme for particle advancement. In one dimension and with finite differencing, we can solve the Poisson equation exactly using a Thomas algorithm (Conte & deBoor 1972), modified for periodic boundaries via the Sherman-Morrison formula (Press et al. 1992). We discuss the details of our scheme for solving the scalar field and scale factor in the appendix.

For all calculations, we used $\Omega_m = 0.26$, $\Omega_\Lambda = 0.74$, and $H_0 = 100 h = 71 \text{ km s}^{-1} \text{ Mpc}^{-1}$. All runs took place in a one-dimensional box of length $10 h^{-1} \text{ Mpc}$ per side, with 65,536 particles to represent the dark matter and 8,192 zones for the Poisson solver and the scalar field. Since we used finite-differencing when forming the gradient to construct the fifth force, we required a large particle-zone ratio to dampen noise in the density field, which couples to the scalar field.

All simulations used the same initial conditions. We distributed particles evenly throughout the grid (described by position $q_i \equiv i\Delta x$) and perturbed them using the Zel'dovich approximation:

$$x = q + \frac{2}{5}aA \sin(kq) \quad (16)$$

$$v = \frac{2}{5}\dot{a}A \sin(kq), \quad (17)$$

where $k = 2\pi/\lambda$ is the comoving wavenumber of the perturbation. The amplitude A can be written in terms of the redshift z_c of the formation of the first caustic:

$$A = -5(1 + z_c)/(2k). \quad (18)$$

Label	α	$K(G^{1+\alpha/2}/H_0^2)$	$\phi_{\text{init}}(G^{1/2})$	$\phi_0(G^{1/2})$
A	-2	0.03	1.89	1.72
B	-2	0.0057	4.02	3.94
C	6	2.0	1.80	1.68
D	6	280.0	3.89	3.83

TABLE 1
SIMULATION PARAMETER CHOICES.

We chose the initial perturbation amplitude such that the first caustic would form at $z_c = 5.0$ for an $\Omega_m = 1.0$ universe, and we chose the comoving wavelength of perturbations to be $\lambda = 10 h^{-1} \text{ Mpc}$. These choices are arbitrary, but commonly used in the literature. All computations start at a redshift of $z = 50$ with DM particle masses determined by equation (9).

We do not know the initial conditions of ϕ in advance, so we must guess initial conditions and iterate until we meet the condition $\dot{a} = H_0$ at the present epoch. Based on the comments made by Farrar and Peebles, we chose four combinations of the potential parameters K and α that yield reasonable behavior. Table 1 lists the parameters, the guessed initial field value at $z = 50$, and the field value today as calculated from equation (4). We performed these calculations in perturbation theory. We selected these parameters for behaviors that were consistent with current observations, but provided unique evolutions of the scalar field for comparison.

3. ANALYSIS OF EFFECTS IN PERTURBATION THEORY

We now illustrate the effects of these additional interactions on structure formation. To highlight each individual consequence of the DM-DE interaction, we separately analyze the resulting structure when including the effects of the variable mass, the modified Hubble drag, the fifth force, and the dynamical field. Finally, we will examine the final structure when these effects are combined. In all that follows, we highlight the behavior when using the potential parameters $K = 0.03$ and $\alpha = -2$ (parameter set A) as an example.

Figure 1 shows the evolution of η , γ , β_{pert} , and δ as functions of scale factor for parameter set A. On average, the fifth force is about three percent of the gravitational force. We expect the fifth force to play a significant role throughout cosmic history. The Hubble drag is reduced by about one percent. The particle mass starts at ten percent greater than its present-day value, but by a scale factor of 0.5 it is only two percent larger. We expect the modified mass to contribute to structure mostly in the early universe, but by the present day its effects will not be significant. In the early universe, the dynamic field gives a large Ω_Λ , and hence a more rapid expansion, which should delay caustic formation relative to standard cosmology. Notice that our calculations do not give precisely the required values of Ω_Λ , but are less than two percent off. We fixed our field at late times such that the energy density of the field was purely in the potential, when in reality the kinetic term, while very small, is not entirely negligible. Fortunately, this small error does not in any way significantly alter structure formation.

We show the density profile at $z = 0$ in Figure 2, modified by the individual additional effects of the DM-DE interaction. We do not show the result from an evolving mass and dynamical field, because these profiles are hard to distinguish from standard cosmology. When iso-

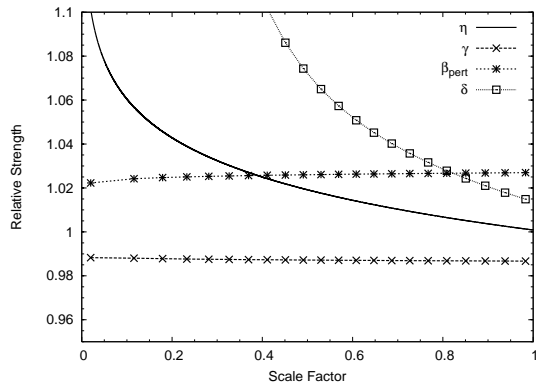


FIG. 1.— Comparison of additional effects due to the DM-DE interactions. Shown are relative values defined above as η (solid line), γ (line with hatches), β_{pert} (line with stars), and δ (line with boxes). The symbols are only to aid in distinguishing the lines.

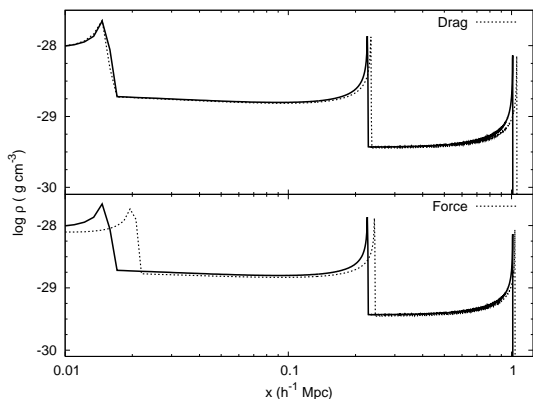


FIG. 2.— Dark matter density profile at $z = 0$. The solid line in all plots is the standard cosmology. The dotted line indicates the effects of the additional interactions: the top panel shows only the result with the drag term included, and the bottom panel shows only the fifth force included. Here, x is the distance from the midplane of each pancake. The numerical shot noise in the density near $x = 1$ is negligible and unimportant.

lating the individual effects of the drag, fifth force, and dynamic field, we forced the scalar field to evolve as if the scale factor obeyed the modified Friedmann equation in equation (6); however, the actual scale factor evolved according to concordance cosmology in these comparisons. We did this because without the dynamic mass in the Friedmann equation, the scalar field would not reach its required value today.

We can easily understand the modifications due to the fifth force: an additional attractive force causes the caustics to form earlier, and hence each peak in the density profile at $z = 0$ is farther away from the center. The effect on each peak is similar: a fifth force only in the early universe will affect mostly the first two caustics, but since the force ratio remains roughly constant even in late times, the latest peak also shifts. The overall size of the pancake is then larger.

Due to the modified drag term alone, the first two caustics form earlier, but the latest caustic forms at the same time as in standard cosmology. This requires more explanation. The Hubble drag term is most important in the early universe. Due to the reduced drag, particles move faster, and reach a greater turnaround radius. So the first two caustics form earlier for the modified cosmology. However, at later times, the drag is no longer

significant, and the third caustic forms at nearly the same redshift as in standard cosmology. Also, it appears that modifications to the drag are very important: even small deviations in the redshift of caustic formation lead to significant difference in the final peak locations.

The increased mass creates tension between two opposing influences on structure formation. Since the particles already in halos are more massive, they create a deeper potential well and encourage other particles to fall in faster, thereby causing caustics to form earlier. On the other hand, a larger Ω_m in the Friedmann equation accelerates the expansion in the early universe, which increases the Hubble drag and dampens structure formation. We found that the expansion effect dominates, but not significantly, and caustics form only slightly later than in standard cosmology. Also, since the DM particle is more massive in the past, the regions near early-forming caustics have a higher density, but by $z = 0$ the mass is the same as in standard cosmology, so the overall amplitude of the density profile does not change.

We must contrast this evolving-mass universe with a Λ CDM cosmology having simply a larger Ω_m . In such a universe, the competing effects of increased mass roughly cancel each other out, and caustics form at similar redshifts to those in standard Λ CDM. In an evolving-mass universe, however, as the mass decreases, the halo potential wells get shallower, but the universe has already expanded more, so outlying particles take longer to reach the halo, and caustics correspondingly form later. At lower redshifts, the particle masses are nearly their present-day values, so this effect is not as significant, and the final peak locations are slightly closer to the pancake midplane.

Finally, the dynamic field has the expected result: more rapid early-universe expansion pulls particles away from each other, and caustics take longer to form. As expected, this effect is nearly negligible in the late universe, as the field approaches its present-day value. Unlike the differences between an evolving-mass universe and a constant-mass universe, the structure modifications from a dynamic field are, in this case, nearly indistinguishable from a universe with a roughly ten percent larger, but still constant, Ω_Λ .

We can also examine the effects on particle velocities due to these additional interactions. Figure 3 is a DM particle phase plot at $z = 0$ with modifications due to the reduced Hubble drag and the fifth force, compared to standard cosmology. The dynamic field and variable mass terms have no effect, but as expected, the reduced drag and fifth force increase particle velocities.

When we combine results, in Figure 4, we see that the effects of the modified mass and the dynamic field tend to cancel out the fifth force. So, the final density profile most closely resembles the results from the drag term alone. The innermost caustic is the same distance from the midplane of the pancake, but the outermost and middle peaks are roughly 15% farther away. The slope of the density profile remains undisturbed and the total number of peaks formed by the present epoch are the same.

4. THE VALIDITY OF PERTURBATION THEORY

So far, we have only considered perturbation theory, relying on a single value to describe the DE scalar field

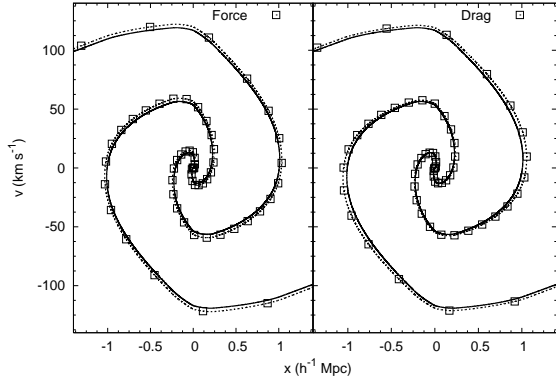


FIG. 3.— Dark matter particle phase plots at $z = 0$. The solid line in all plots is from concordance cosmology, and the dotted lines with open squares are the results from including the effects indicated in each plot. The open squares only represent select data points, to aid in distinguishing the lines. We have omitted the plots with dynamic field and dynamic mass effects, since these have no discernible influence.

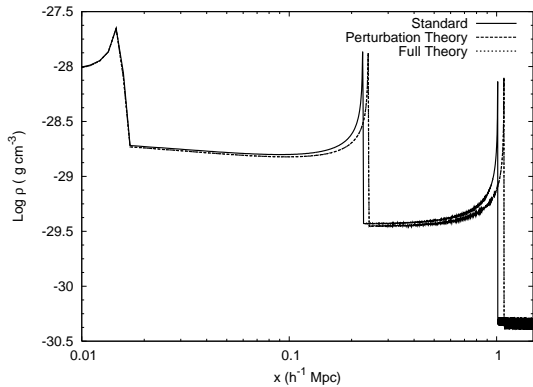


FIG. 4.— Dark matter density profile at $z = 0$. The solid line is from standard cosmology. The dashed line is the density from using perturbation theory, and the dotted line is from using full theory. This is including all effects. Note that perturbation theory is nearly indistinct from the full theory. The numerical shot noise in the density near $x = 1$ is negligible and unimportant.

at a specific time. When we relax this constraint, each particle feels its own force, has its own drag, and has an independent mass. When solving the Friedmann equation, we must take a spatial average of the field, rather than using a single background value. Also, the expression for the fifth force changes to be directly proportional to gradients in the scalar field.

There is some ambiguity when considering the initialization of the scalar field. While the average value must match the perturbation theory background value, we are left with few clues to the initial wavelength and amplitude of the perturbations. So, using adiabatic reasoning, we initialized ϕ to have the same spectrum as the density field, which in our case is a single perturbation mode with wavelength $\lambda = 10h^{-1}$ Mpc at $z = 0$. However, we freely chose the amplitude, and we found that to make an attractive fifth force, which is required for a Yukawa-type interaction, we needed ϕ to have a phase opposite to that of the density field.

We must take care in the initialization of both the background value and amplitude of perturbations of the field when considering the full theory. First, the addition of the gradient term in the equation of motion for the field will affect the field's background evolution, and

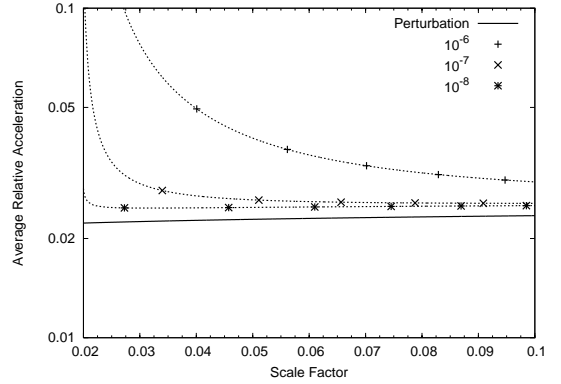


FIG. 5.— Average ratio of fifth force to gravitational force ($\langle\bar{\beta}\rangle - 1$) for perturbation theory (solid line), compared to the full result with varying initial amplitudes (dotted lines with various marks, labeled in figure). The marks on the lines only represent select data points, to aid in distinguishing the lines. Shown are the average strengths up to the given scale factor.

may force us to modify the initial value, so that ϕ still satisfies the present-day condition in equation (7). Fortunately, the gradients are not large, and this term does not modify the evolution of ϕ greatly. Hence, we constructed the field so its average value matched the background perturbation value. It appears that perturbation theory is perfectly appropriate for probing the linear results of this model, such as estimates of the Hubble time and the location of peaks in the CMB power spectrum, which Farrar and Peebles discuss.

Secondly, by varying the initial amplitude, we can change the strength of the fifth force at high redshift. Kesden & Kamionkowski (2006a,b) have shown that a constraint on any dark matter fifth force to within only a few percent of the gravitational force is observationally possible. The fifth force under perturbation theory agrees with this constraint: $\beta_{pert} \approx 1.03$ throughout cosmic history. Figure 5 shows the space-averaged and time-averaged value of $\beta_{pert} - 1$ and $\beta - 1$, which we denote as $\langle\bar{\beta}\rangle - 1$, versus redshift for varying initial amplitudes. This is the average fraction of gravitational acceleration experienced by the DM particles due to the fifth force up to the given scale factor. The field fluctuates rapidly in the early universe, and by time-averaging we can better examine the general force trends. The fluctuations in the field decay rapidly and asymptotically approach a constant value by redshift $z = 45$.

No matter the initial amplitude, the average perturbation theory fifth force ratio agrees to within ten percent with the full result by the present epoch. However, the strength of the fifth force matters much more at high redshifts: different forces here can greatly affect structure formation. We found that an initial amplitude contrast of $\delta\phi(z = 50) = 10^{-8}$ provides roughly the same order of magnitude additional acceleration as perturbation theory predicts at early times.

For amplitudes smaller than 10^{-8} , the results for the fifth force do not change. Since the scalar field couples directly to the dark matter density, the field will always contain perturbations. If we initialize the amplitudes below the threshold of 10^{-8} , the density coupling will produce fluctuations in the scalar field spectrum, creating a fifth force. However, larger amplitudes provide too much of an acceleration at early times. For example, a contrast

of $\delta_\phi(z=50) = 10^{-6}$ provides an average fifth force that is almost half as strong as gravity at early times. We found that if the initial contrast is larger than can be handled adequately by perturbation theory, then we get radically different structure formation, such as a very early first caustic and the development of four caustics by the present epoch. Note that these results are largely redshift-independent: the DM coupling will always end up dominating the spectrum of scalar field fluctuations after a short period of time. The large fifth force for amplitudes above 10^{-8} is due to the large artificial initial scalar field amplitude.

However, if the amplitude of perturbations is small in the early universe, then perturbation theory under-emphasizes the fifth force at high redshift. The fact that perturbation theory cannot describe large fluctuations makes sense. However, we would expect that perturbation theory should accurately capture the behavior of all initial amplitudes below a certain value.

With the above considerations, we examined the case of an initial contrast of $\delta_\phi(z=50) = 10^{-8}$, since this provides a fifth force large enough to affect structure, but which is not ruled out by observations. We compare perturbation theory to the results from a full dynamical field. We found that for this amplitude, perturbation theory is excellent in capturing the structure and evolution of halos. By construction, the average value of the dynamical field is the same as the background field in perturbation theory. Hence, the modified drag term and modified mass terms are almost identical. Also, perturbation theory appears to be adequate for describing the evolution of the scalar field, so the effects of the dynamic field itself agree in the full theory. Additionally, since fluctuations dampen with time, we only need to satisfy perturbation theory constraints in the early universe. We see in Figure 4 that, for this particular amplitude of fluctuations, perturbation theory is excellent in describing the overall structure of the pancakes.

Overall, as Figure 4 showed, perturbation theory seems to be adequate in describing the larger features of the pancakes: the number of caustics and the location of all three caustics at $z=0$. With the notable exception of the fifth force, as we decrease initial scalar field amplitudes, perturbation theory becomes more accurate in providing an accurate solution. Even though the perturbation theory fifth force disagrees with the full theory by several percent, this is not enough to affect structure formation at our resolution.

It is interesting to note that we can produce significant changes in structure formation even with a negligible fifth force, such as might happen with a sufficiently screened potential. Figure 6 shows the results from the full theory, but with no fifth force. In this case, we get stronger deviations in the innermost pancake substructure. Also, the second caustic forms slightly later than in standard cosmology, while the largest caustic is no different than when the fifth force is large.

5. DISTINGUISHABILITY OF MODELS

The models chosen in Table 1 are constructed to be consistent with current observations. For example, all these models predict values for the CMB peak locations that are within observational constraints.

Figure 7 shows how each of our chosen potential pa-

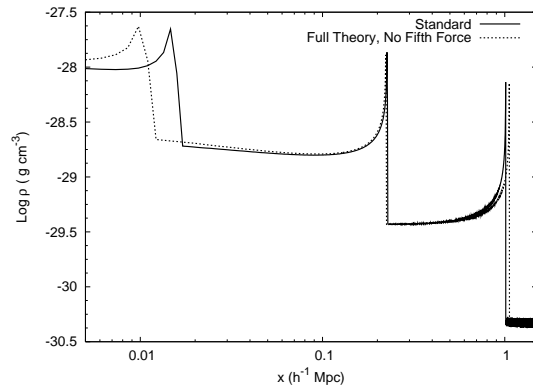


FIG. 6.— Dark matter density profile at $z=0$. The solid line is the standard Λ CDM cosmology, and the dashed line is the final result in full theory when the fifth force is negligible. The numerical shot noise in the density near $x=1$ is negligible and unimportant.

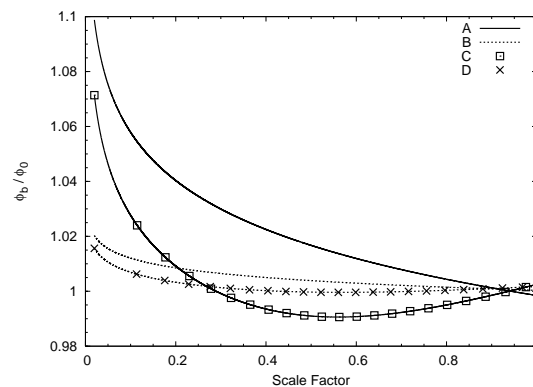


FIG. 7.— Evolution of ϕ_b , relative to the present-day value, for the various potential parameters labeled in Table 1. Note that the symbols are only to aid in distinguishing the lines. These calculations are from perturbation theory.

rameters in Table 1 affects the evolution of ϕ . These results agree with the perturbation results from Farrar and Peebles. There are in general two classes of viable ϕ evolution tracks. We see from Table 1 that models such as A and C have a smaller initial value, but drop by roughly ten percent by the current epoch. On the other hand, models such as B and D have a high initial value and do not change much throughout cosmic history.

These two classes of parameter sets have interesting consequences for the behaviors of the DM particle mass, the modified Hubble drag, the fifth force, and the dynamical field itself. Figure 8 shows how the mass ratio (η), the modified Hubble drag (γ), the fifth-force acceleration (β_{pert}), and the field energy density ratio (δ) vary across the models in perturbation theory. For models of the second type, in which ϕ does not change much, the mass at $z=50$ is much closer to its present-day value, and hence this effect on structure formation will be smaller than in models where ϕ varies strongly. Also, if ϕ does not vary much, then the Hubble drag will not be modified greatly. Together, this makes sense: a set of parameters that favors a slightly-varying scalar field will look more like standard Λ CDM than those which do not. Finally, for larger values of ϕ , the fifth force is much weaker, since the force is proportional to ϕ^{-2} in perturbation theory.

These behaviors play out accordingly in the final structure at $z=0$, as Figure 9 shows. These calculations were done using the full theory. When performing the analysis

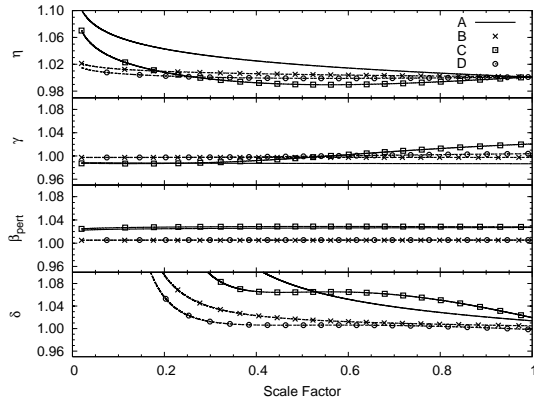


FIG. 8.— Evolution of mass (η), Hubble drag (γ), fifth-force acceleration (β_{pert}), and dynamical field (δ) for the various potential parameters labeled in Table 1. The symbols are only to aid in distinguishing the lines. These calculations are from perturbation theory.

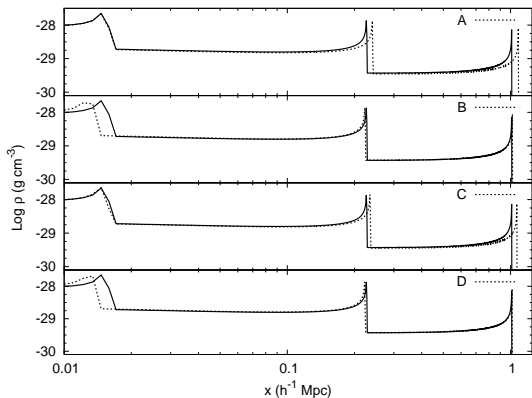


FIG. 9.— Dark matter density profile at $z = 0$. The solid line in all plots is the standard cosmology. The dashed line indicates the result in full theory, for the various potential parameters labeled in Table 1.

in the full dynamical theory, we again have to be careful when setting the initial scalar field amplitude. For all cases, we set an initial contrast of $\delta\phi(z = 50) = 10^{-8}$.

Models *B* and *D* do not differ much from standard cosmology or each other. Models *A* and *C*, while both different from Λ CDM, remain mostly indistinguishable, except that parameter set *A*, whose changes in ϕ are most drastic, produces caustics that are slightly farther away from the pancake midplane. Even though ϕ is increasing at the present epoch in parameter set *C*, this change happens at late times, and so it does not have a significant effect on the resulting structure.

We also performed this study in perturbation theory, and we found that accounting for the effects of the full dynamics do not increase the distinguishability of the models.

Surprisingly, we do notice some additional distinguishing features when examining the phase plots, as in Figure 10. Since models *B* and *D* remain nearly identical to concordance cosmology, we do not display them. While models *A* and *C* share many common features, the drag term γ increases at late times in model *C*. This eventually slows down particles at low redshifts and pushes the peak velocities closer to concordance cosmology. Hence, the higher peak particle velocities distinguish model *A*, whereas simply considering pancake density profiles may not.

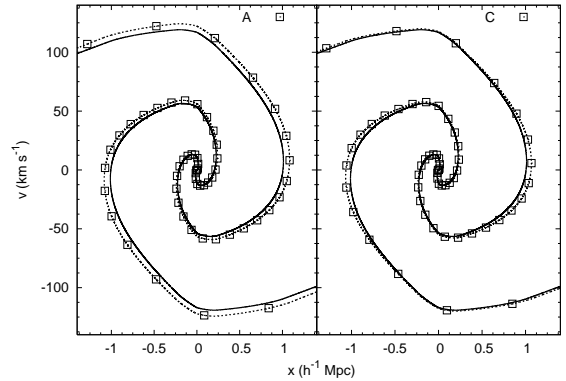


FIG. 10.— Dark matter particle phase plots at $z = 0$. The solid line in all plots is from concordance cosmology, and the dotted lines are the results from various model parameters, which are labeled in the plots. These were calculated in the full theory. The symbols are only to aid in distinguishing the lines.

6. CONCLUSIONS

These one-dimensional simulations have clearly demonstrated that models of interacting dark matter and dark energy affect the growth and structure of plane parallel perturbations. Various consequences of these theories play important roles at different stages in halo evolution. Larger fifth forces and modified Hubble drag terms in the high-redshift universe greatly alter early structure formation, while an evolving particle mass can affect even late-forming structures. Ordinary quintessence, which is a dynamic field alone, does not significantly alter the formation of pancakes. Of all the effects, a modification to the Hubble drag gives the largest deviations in the resulting structure.

We have found that models that are specifically tuned to match current observational constraints, such as the CMB peak locations and equation of state parameters, produce significant deviations from standard Λ CDM in the formation of pancakes.

We have also found that an approach based on perturbation theory is adequate for understanding the general evolution of the scalar field. However, perturbation theory does not seem to be appropriate at high redshift. Even for arbitrarily small amplitudes, the fifth force in the full theory is larger than that obtained by perturbative techniques. This behavior deviates from the general pattern of perturbation methods, in that it does not accurately describe all characteristics for amplitudes smaller than a threshold value.

This discrepancy arises from the fact that the fifth force directly depends on the gradient of the field. In the perturbative method described by Farrar and Peebles, the kinetic terms of the perturbation field equation of motion are dropped, producing a Poisson equation for the perturbation field and leading to the simplification of the fifth force expression found in equation (14). This simplification is valid at low redshifts, but at high redshifts the kinetic terms are still important. Thus, any realistic spectrum of perturbations for the scalar field which ignores the kinetic terms may be invalid for the very largest-scale perturbations. It also appears that the initial scalar field amplitude does not serve as a suitable “small” parameter for governing the appropriateness of perturbation theory.

Because we can freely choose the initial amplitude, full

theory gives us more freedom to study the effects of various strengths of a fifth force. In the context of this model, this can also work in reverse: working within these frameworks, constraints on a fifth force in the dark sector could lead to limitations on the amplitudes of a DE scalar field in the early universe.

Anninos and Norman have extensively studied the effects on baryons in the formation of pancakes (Anninos & Norman 1994; Anninos et al. 1995). While baryons appear to modify only the last-forming caustic, DM-DE interactions affect all caustics. Hence, the modifications to the last caustic may be masked by the baryon dynamics. Also, baryons do not appear to significantly modify dark matter particle velocities, while some of the models considered above produce significant variations.

The structural differences described above are relatively small. However, in three dimensions these effects should appear as percent-level differences in the statistical properties of large samples of dark matter halos. The various effects could produce different halo mass functions, which could be compared to other high-resolution mass functions, such as the Λ CDM ones considered by Warren et al. (2006). In fact, Mainini & Bonometto (2006) have shown that DM-DE interactions do modify analytic mass functions, and a direct simulation could be compared against these results. DM-DE interactions may also affect halo substructure, in which case they would impact NFW profiles (Navarro et al. 1997) and distributions of concentrations in halo catalogs (Lukic et al. 2007; Reed et al. 2003).

The present work focused on a single model and a single potential, simply to analyze the feasibility of a direct simulation approach. With a full three-dimensional simulation, we can also examine the results of using other potentials, or even more complicated models. With future simulations, we can also contrast these structure formation results to the N -body results from other theories of DE, such as modified General Relativity, which have been examined in Stabenau & Jain (2006).

For the models with the largest deviations from Λ CDM, we notice that the sign of the difference of the caustic peak location changes. This implies that the shape and evolution of the mass function for these cosmologies will change relative to Λ CDM, not simply the amplitude. This holds the most hope for observations, particularly for surveys such as the DES (Annis et al.

2005). Most notably, we found that we will still get significant modifications to pancake structure even if the fifth force is negligible. Indeed, the modifications to the mass function may even be more significant without a fifth force. Since many recent efforts have concentrated mostly on constraining the fifth force (Kesden & Kamionkowski 2006a; Farrar & Rosen 2007; Bertolami et al. 2007; Guo et al. 2007), this result clearly shows that we should not ignore the other consequences, such as modifications to the Hubble drag, of these models. Also, the phase plots revealed another observable effect: the large-scale matter velocity field, which is also accessible to the DES survey. The feasibility of constraining these models with this behavior could be tested with velocity correlations in full three-dimensional simulations.

However, there are several computational and theoretical challenges in developing and analyzing full three dimensional simulations. For example, there should be a stronger theoretical understanding of the initial conditions of the field. While implicitly solving the scalar field is relatively straightforward in one dimension, requiring a simple Thomas algorithm, a full three dimensional solver would be much more complex, probably requiring a multigrid solver that could easily be combined with existing parallel adaptive-mesh codes such as FLASH (Fryxell et al. 2000) or GADGET-2 (Springel 2005). Since there might be interesting changes in halo substructure, simulations will require very high resolution. Also, simulations will require many halos to get significant statistical results.

Fortunately, none of these issues are intractable, and this approach holds much hope for providing a strong, consistent method of analyzing the nonlinear effects of these myriad dark energy models.

The authors would like to thank Luke Olson, Ben Wandelt, and Greg Huey for enlightening and valuable discussions.

The authors acknowledge support under a Presidential Early Career Award from the U.S. Department of Energy, Lawrence Livermore National Laboratory (contract B532720). Additional support was provided by a DOE Computational Science Graduate Fellowship (DE-FG02-97ER25308) and the National Center for Supercomputing Applications.

APPENDIX

NUMERICALLY SOLVING THE SCALAR FIELD EQUATION

We have

$$\ddot{\phi} - \frac{c^2}{a^2} \nabla^2 \phi + 3 \frac{\dot{a}}{a} \dot{\phi} + \frac{dV}{d\phi} + \frac{\rho}{\phi} a^{-3} = 0. \quad (\text{A1})$$

We will let $V(\phi) = K\phi^{-\alpha}$, and we have re-introduced c for clarity. We may break up equation (A1) using standard operator splitting techniques:

$$\phi^n \rightarrow \phi^{(1)} : \frac{\partial^2 \phi}{\partial t^2} - \frac{c^2}{a^2} \nabla^2 \phi = 0 \quad (\text{A2})$$

$$\phi^{(1)} \rightarrow \phi^{n+1} : \frac{\partial^2 \phi}{\partial t^2} + \frac{dV}{d\phi} + 3 \frac{\dot{a}}{a} \frac{\partial \phi}{\partial t} + \frac{\rho}{\phi} a^{-3} = 0. \quad (\text{A3})$$

Here and below, superscripts are temporal indices and subscripts will denote the index of the location on the mesh.

We solve Eq.(A2) by reducing it to a set of two 1st-order equations:

$$\frac{\partial \phi^{(1)}}{\partial t} = \dot{\phi}^n \quad (\text{A4})$$

$$\frac{\partial \dot{\phi}^{(1)}}{\partial t} = -\frac{c^2}{a^2} \nabla^2 \phi^n. \quad (\text{A5})$$

Since the sound speed is so high ($v_s = c/a$), we found that a direct integration scheme was highly unstable except for unworkably small Δt . So, we use a midpoint method for Eq.(A4) and a fully implicit method for equation (A5) :

$$\phi_i^1 = \phi_i^n + \frac{1}{2} \Delta t \left(\dot{\phi}_i^n + \dot{\phi}_i^{(1)} \right) \quad (\text{A6})$$

$$\dot{\phi}_i^{(1)} = \dot{\phi}_i^n + \frac{c^2 \Delta t}{\Delta x^2 (a^{(1)})^2} \left(\phi_{i+1}^{(1)} - 2\phi_i^{(1)} + \phi_{i-1}^{(1)} \right). \quad (\text{A7})$$

We substitute our expression for $\phi_i^{(1)}$ into equation (A7), yielding the matrix equation $Ax = b$, where

$$x_i \equiv \dot{\phi}_i^{(1)}, \quad (\text{A8})$$

$$\begin{aligned} b_i \equiv & \dot{\phi}_i^n + \sigma \phi_{i+1}^n + \gamma \sigma \dot{\phi}_{i+1}^n \\ & - 2\sigma \phi_i^n - 2\gamma \sigma \dot{\phi}_i^n \\ & + \sigma \phi_{i-1}^n + \gamma \sigma \dot{\phi}_{i-1}^n, \end{aligned} \quad (\text{A9})$$

and

$$A = \begin{pmatrix} 1 + 2\sigma\gamma & -\sigma\gamma & 0 & \cdots & -\sigma\gamma \\ -\sigma\gamma & 1 + 2\sigma\gamma & -\sigma\gamma & \cdots & 0 \\ 0 & -\sigma\gamma & 1 + 2\sigma\gamma & -\sigma\gamma & 0 \\ \cdots & \cdots & \cdots & \cdots & \cdots \\ -\sigma\gamma & \cdots & 0 & -\sigma\gamma & 1 + 2\sigma\gamma \end{pmatrix}.$$

Note the periodic boundary conditions. We have defined

$$\begin{aligned} \sigma &\equiv \frac{c^2}{(a^{(1)})^2} \frac{\Delta t}{\Delta x^2}, \\ \gamma &\equiv \frac{1}{2} \Delta t. \end{aligned} \quad (\text{A10})$$

We solved this matrix-vector equation exactly using a Thomas algorithm (Conte & deBoor 1972), modified for periodic boundaries via the Sherman-Morrison formula (Press et al. 1992).

We may now update our solution through equation (A3) by expanding in a Taylor series:

$$\dot{\phi}^{n+1} = \dot{\phi}^{(1)} + \ddot{\phi}^{(1)} \Delta t + \frac{1}{2} \frac{d^3 \phi^{(1)}}{dt^3} \Delta t^2 + O(\Delta t^3), \quad (\text{A11})$$

where

$$\ddot{\phi}^{(1)} = K\alpha (\phi^n)^{-\alpha-1} - 3 \frac{\dot{a}^n}{a^n} \dot{\phi}^{(1)} - \frac{\rho}{\phi^{(1)}} (a^n)^{-3}$$

and

$$\begin{aligned} \frac{d^3 \phi^{(1)}}{dt^3} = & -K\alpha(\alpha+1) (\phi^n)^{-\alpha-2} \dot{\phi}^{(1)} - 3 \frac{\ddot{a}^n}{a^n} \dot{\phi}^{(1)} \\ & + 12 \left(\frac{\dot{a}^n}{a^n} \right)^2 \dot{\phi}^{(1)} - \frac{\dot{\rho}}{\phi^{(1)}} (a^n)^{-3} \\ & - \frac{\rho}{(\phi^{(1)})^2} (a^n)^{-3} \dot{\phi}^{(1)} + 3 \frac{\rho}{\phi^{(1)}} (a^n)^{-4} (\dot{a}^n). \end{aligned}$$

Here, $\dot{\rho} = (\rho^n - \rho^{n-1}) / dt$.

At any step n , after computing ϕ^n across the grid, we may update the scale factor using a Taylor series:

$$a^{n+1} = a^n + \dot{a}^n \Delta t + \frac{1}{2} \ddot{a}^n \Delta t^2 + O(\Delta t^3), \quad (\text{A12})$$

where \dot{a} and \ddot{a} are given by the Friedmann equation and Friedmann energy equation, respectively:

$$\dot{a}^n = \left[H_0^2 \Omega_m \frac{\bar{\phi}}{\phi_0} a^{-1} + \frac{8\pi G}{3} a^2 \rho_\phi \right]^{1/2} \quad (\text{A13})$$

$$\ddot{a}^n = -\frac{1}{2} H_0^2 \Omega_m \frac{\bar{\phi}}{\phi_0} a^{-2} - \frac{4\pi G}{3} (1 + 3w) \rho_\phi a. \quad (\text{A14})$$

Ignoring fluctuations, the equation of state parameter, w , is

$$w \equiv \frac{p_\phi}{\rho_\phi} = \frac{\frac{1}{2}\bar{\phi}^2 - V(\bar{\phi})}{\frac{1}{2}\bar{\phi}^2 + V(\bar{\phi})}. \quad (\text{A15})$$

REFERENCES

- Alcaniz, J. 2006, *Braz.J.Phys.*, 36, 1109, astro-ph/0608631
- Amendola, L. 2000, *Phys. Rev. D*, 62, 043511
- Amendola, L., Campos, G. C., & Rosenfeld, R. 2007, *Phys.Rev.D*, 75, 083506
- Amendola, L. & Tocchini-Valentini, D. 2001, *Phys. Rev. D*, 64, 043509
- Anninos, W. Y. & Norman, M. J. 1994, *ApJ*, 429, 434
- Anninos, W. Y., Norman, M. L., & Anninos, P. 1995, *ApJ*, 450, 1
- Annis, J. et al. 2005, astro-ph/0510195
- Bean, R., Carroll, S., & Trodden, M. 2005, astro-ph/0510059
- Bertolami, O., Pedro, F. G., & Delliou, M. L. 2007, astro-ph/0705.3118
- Conte, S. & deBoor, C. 1972, *Elementary Numerical Analysis* (McGraw-Hill, New York)
- Corasaniti, P.-S., Huterer, D., & Melchiorri, A. 2007, *ArXiv Astrophysics e-prints*
- de Bernardis, P. et al. 2000, *Nature*, 404, 955
- Dodelson, S., Kaplinghat, M., & Stewart, E. 2000, *Phys.Rev.Lett.*, 85, 5276
- Doran, M. & Jäckel, J. 2002, *Phys. Rev. D*, 66, 043519
- Farrar, G. R. & Peebles, P. 2004, *Astrophys.J.*, 604, 1, astro-ph/0307213
- Farrar, G. R. & Rosen, R. A. 2007, *Phys.Rev.Lett.*, 98, 171302
- Fryxell, B. et al. 2000, *Astrophys.J. Supp.*, 131, 273
- Gnedin, N. 1993, in *Bulletin of the American Astronomical Society*, Vol. 25, Bulletin of the American Astronomical Society, 1464–+
- Guo, Z.-K., Ohta, N., & Tsujikawa, S. 2007, *Phys. Rev. D*, 76, 023508
- Hockney, R. W. & Eastwood, J. W. 1988, *Computer simulation using particles* (Bristol: Hilger)
- Huey, G. & Wandelt, B. D. 2006, *Phys.Rev.D*, 74, 023519
- Ivezic, Z. 2007, in *American Astronomical Society Meeting Abstracts*, Vol. 210, American Astronomical Society Meeting Abstracts, 66.05
- Kesden, M. & Kamionkowski, M. 2006a, *Phys.Rev.Lett.*, 97, 131303, astro-ph/0606566
- . 2006b, *Phys.Rev.D*, 74, 083007, astro-ph/0608095
- Koivisto, T. 2005, *Phys.Rev.D*, 72, 043516
- Lukic, Z., Heitmann, K., Habib, S., Bashinsky, S., & Ricker, P. M. 2007, *ArXiv Astrophysics e-prints*
- Macciò, A. V., Quercellini, C., Mainini, R., Amendola, L., & Bonometto, S. A. 2004, *Phys. Rev. D*, 69, 123516
- Mainini, R. & Bonometto, S. 2006, *Phys.rev.D*, 74, 043504, astro-ph/0605621
- Manera, M. & Mota, D. F. 2006, *MNRAS*, 371, 1373
- More, J. G. 1988, PhD thesis, AA(Edinburgh Univ. (Scotland).)
- Navarro, J., Frenk, C., & White, S. 1997, *Astrophys.J.*, 490, 493
- Nusser, A., Gubser, S., & Peebles, P. 2005, *Phys.Rev.D*, 71, 083505, astro-ph/0412586
- Olivares, G., Atrio-Barandela, F., & Pavón, D. 2006, *Phys.Rev.D*, 74, 043521
- Peebles, P. & Ratra, B. 1988, *Astrophys.J.Lett.*, 325, L17
- Percival, W. J. et al. 2001, *MNRAS*, 327, 1297
- Perlmutter, S. et al. 1999, *ApJ*, 517, 565
- Press, W., Flannery, D., Teukolsky, S., & Vetterling, W. 1992, *Numerical Recipes in C: The Art of Scientific Computing* (Cambridge University Press)
- Ratra, B. & Peebles, P. 1988, *Phys.Rev.D*, 37, 3406
- Reed, D., Gardner, J., Quinn, T., Stadel, J., Fardal, M., Lake, G., & Governato, F. 2003, *MNRAS*, 346, 565
- Riess, A. G. et al. 1998, *AJ*, 116, 1009
- Springel, V. 2005, *MNRAS*, 364, 1105
- Stabenau, H. & Jain, B. 2006, *Phys.Rev.D*, 74, 084007, astro-ph/0604038
- Valinia, A., Shapiro, P. R., Martel, H., Vishniac, E. T., & Villumsen, J. V. 1995, in *Bulletin of the American Astronomical Society*, Vol. 27, Bulletin of the American Astronomical Society, 1365
- Warren, M., Abazajian, K., Holz, D., & Teodoro, L. 2006, *Astrophys.J.*, 646, 881, astro-ph/0506395
- Yuan, W., Centrella, J. M., & Norman, M. L. 1991, *Astrophys.J.Lett.*, 376, L29
- Zel'dovich, Y. B. 1970, *A&A*, 5, 84
- Zimdahl, W. & Pavon, D. 2001, *Phys. Lett. B*, 521, 133, astro-ph/0105479